Geophysical Research Letters

RESEARCH LETTER
10.1029/2024GL114033

Shear Strain Evolution Spanning the 2020 Mw6.8 Elazığ and 2023 Mw7.8/Mw7.6 Kahramanmaraş Earthquake Sequence Along the East Anatolian Fault Zone

Ziming Liu[1,2], Heng Luo[1], Yann Klinger[2], and Teng Wang[1]

[1]School of Earth and Space Science, Peking University, Beijing, China, [2]Université de Paris Cité, Institut de Physique du Globe de Paris, CNRS, Paris, France

Abstract Shallow creep along strike-slip faults is essential in releasing strain during earthquake cycles. However, its origin—whether inherent or triggered by earthquakes—remains debated. Using Interferometric Synthetic Aperture Radar phase-gradient data, we map shear-strain rates along the East Anatolian Fault Zone (EAFZ) before and after the 2020 Mw6.8 Elazığ and 2023 Mw7.8/Mw7.6 Kahramanmaraş earthquakes. The observed strain-rate distributions strongly correlate with coseismic slips in the EAFZ. The stress-driven afterslip model constrained by the phase-gradient time series reproduces distinct decaying patterns of newly activated creeping segments, showing that rapid afterslip may decay slowly and keep slipping for decades. Our results reveal that large earthquakes can accelerate, expand, and trigger shallow fault creep, highlighting the roles of fault frictional properties and stress changes caused by nearby earthquakes. These findings provide new insights into fault creep mechanisms and their linkage to large earthquakes, with implications for faulting behaviors.

Plain Language Summary Understanding the silent slips of large-scale strike-slip faults and their connection with nearby earthquakes is crucial for elucidating the mechanisms and causes of shallow creep, a topic that remains debated. Interferometric Synthetic Aperture Radar is a powerful tool for mapping millimeter-level deformation and its spatial variation, that is, strain across faults with high spatial resolution. Here, we map and investigate the strain distribution of the East Anatolian Fault Zone from 2014 to 2023, with different periods spanning three significant earthquakes: the 2020 Mw 6.8 Elazığ earthquake and the 2023 Mw 7.8 and Mw 7.6 Kahramanmaraş earthquake sequence. The shear-strain rates and the postseismic phase-gradient time series clearly depict the spatial and temporal distribution of shallow slip before and after these earthquakes. Our results show a strong correlation between shallow slip and earthquakes, revealing how fault frictional properties and changes in seismic stress influence afterslip behavior. Simulation outcomes provide compelling evidence that afterslip triggered by earthquakes may continue for decades.

Key Points:

- We map the shear strain rates from the Interferometric Synthetic Aperture Radar phase gradient spanning two recent large earthquakes on the East Anatolian Fault
- The shear-strain rates and coseismic slip models show that earthquakes can initiate, extend, and accelerate shallow creep
- Stress-driven afterslip model constrained by time-series phase gradients reveals earthquake-triggered creep may continue for decades

Supporting Information:

Supporting Information may be found in the online version of this article.

Correspondence to:

T. Wang,
wang.teng@pku.edu.cn

Citation:

Liu, Z., Luo, H., Klinger, Y., & Wang, T. (2025). Shear strain evolution spanning the 2020 Mw6.8 Elazığ and 2023 Mw7.8/Mw7.6 Kahramanmaraş earthquake sequence along the East Anatolian Fault Zone. *Geophysical Research Letters*, *52*, e2024GL114033. https://doi.org/10.1029/2024GL114033

Received 4 DEC 2024
Accepted 28 FEB 2025

Author Contributions:

Conceptualization: Teng Wang
Data curation: Ziming Liu, Heng Luo
Formal analysis: Ziming Liu
Funding acquisition: Teng Wang
Investigation: Ziming Liu, Heng Luo
Methodology: Ziming Liu
Resources: Yann Klinger
Software: Ziming Liu, Heng Luo
Supervision: Yann Klinger, Teng Wang
Writing – original draft: Ziming Liu
Writing – review & editing: Heng Luo, Yann Klinger, Teng Wang

1. Introduction

Creep in the uppermost crust is a commonly observed phenomenon on many strike-slip faults with different tectonic settings, including the San Andreas Fault (e.g., Jolivet et al., 2015; Steinbrugge et al., 1960), North Anatolian Fault (NAF) (e.g., Bilham et al., 2016; Cakir et al., 2005; Rousset et al., 2016), Haiyuan Fault (e.g., Cavalié et al., 2008; Jolivet et al., 2012), etc. Interseismic creep and transient afterslip are two types of creep observed at different stages of the earthquake cycle; both slip aseismically and play crucial roles in releasing the accrued strain at shallow depths (e.g., above 5 km) (Scholz, 1998). Therefore, the spatial extent and temporal behavior of shallow creep are closely associated with the potential of large earthquakes, offering valuable information for the understanding of faulting behaviors.

The underlying mechanism of shallow creep is linked to faults' steady-state, velocity-strengthening behavior, as described by the rate- and state-dependent friction (RSF) law (Dieterich, 1979; Ruina, 1983). Based on this mechanism, there are two main perspectives on the interseismic fault creep (Harris, 2017): One view suggests that fault creep observed alongside large earthquakes may be residual from these seismic events (Cakir et al., 2005, 2012; Cetin et al., 2014); The other view suggests that much of the creep observed today results from ongoing tectonic loading (Bilham et al., 2016; Hussain et al., 2016). With afterslip models constrained by current slip rates near the 1868 M6.8 Hayward earthquake, it is argued that the derived creep rate is too high to be real in the late 1800s, precluding its origin from afterslip (Langbein et al., 2006; Perfettini & Avouac, 2004). On the other hand, Liu and Wang (2023) derive the creep distributions from high-resolution shear-strain rates along the NAF,

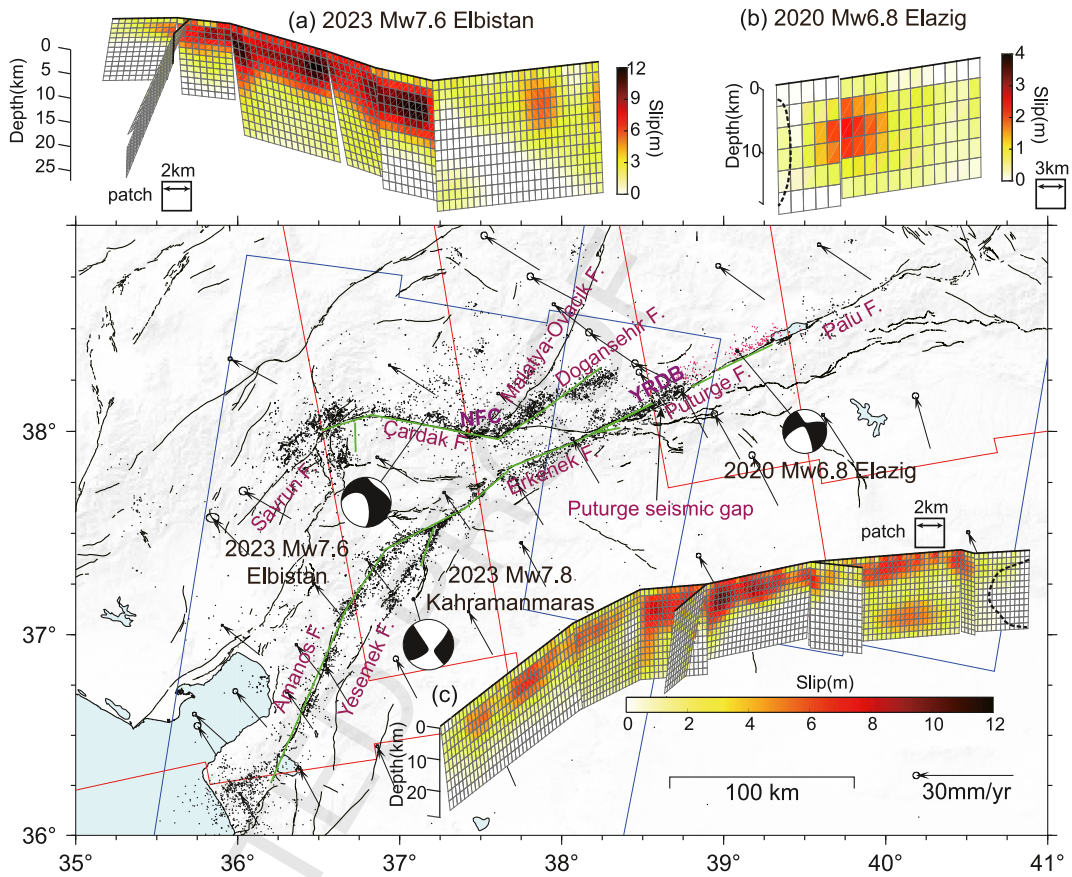

Figure 1. Tectonic setting of the East Anatolian Fault Zone and slip distribution of the 2020 Mw6.8 Elazığ and 2023 Mw7.8/Mw7.6 Kahramanmaraş earthquake sequence. Black solid lines represent active faults in the region (Emre et al., 2013). Three beach balls show the focal mechanisms of the earthquakes from USGS. Black arrows indicate the velocities from the GNSS network (England et al., 2016) in a fixed Eurasian plate frame. Red and blue boxes indicate the ascending and descending tracks of Sentinel-1 satellites, respectively. Green solid lines and black dots represent the surface ruptures and aftershocks of the 2023 Turkey earthquake doublet (Lomax, 2023). Pink dots represent the aftershocks of the 2020 Elazığ earthquake (Melgar et al., 2020). (a–c) Present coseismic slip distributions of the 2023 Mw7.6 Elbistan earthquake, the 2020 Mw6.8 Elazığ earthquake (Pousse-Beltran et al., 2020), and the 2023 Mw7.8 Kahramanmaraş earthquake, respectively. Black dashed lines in panels (b, c) indicate the approximate location of the Puturge seismic gap.

revealing a tight link between shallow fault creep and past earthquakes. However, since the studied NAF earthquakes occurred at least 15 years before the Interferometric Synthetic Aperture Radar (InSAR) acquisition, direct observations of aseismic slip before and immediately after these events are absent, hindering our understanding of how earthquakes interact with their adjacent creeping segment.

The East Anatolian Fault Zone (EAFZ) features a 700-km-long left-lateral strike-slip fault between the Anatolian and Arabian plates, with a slip rate of ∼10 mm/yr (Reilinger et al., 2006; Taymaz et al., 2004). Unlike the NAF, which experienced significant seismic activities in the 20th century, the EAFZ has been largely quiet since the 19th century (Duman & Emre, 2013; Provost et al., 2024). Recently, the 2020 Mw6.8 Elazığ earthquake ruptured part of the main branch of the EAFZ, breaking half of the Pütürge seismic gap, which has not been ruptured in the past several hundred years (Duman & Emre, 2013) (Figure 1). Three years later, the 2023 Mw 7.8 Kahramanmaraş earthquake initiated on a splay fault and ruptured a ∼300 km long segment of the main EAFZ. The rupture then propagated along the Amanos segment to the south and the Ekenek fault to the northeast until it stopped at ∼30 km southeast of the 2020 Mw6.8 earthquake. Following the Mw7.8 event, an Mw7.6 earthquake struck the Çardak fault and ruptured a ∼150 km long northern branch of the EAFZ along the Savrun, Çardak, and Doğanşehir segments (Ezgi Güvercin, 2024; Karabulut et al., 2023; Ren et al., 2024; Zhang et al., 2023). These recent earthquakes offer a unique opportunity to explore the behaviors of shallow creep before, during, and shortly after large strike-slip earthquakes.

Here, we use the InSAR phase-gradient stacking to map the strain rates of the EAFZ before and after the 2020 and 2023 earthquakes with high resolution. With shear-strain rates along the entire EAFZ, we investigate how the earthquakes affected the shallow creep from 2014 to 2023. Furthermore, we conduct a phase-gradient time-series analysis to obtain the evolution of the new creeping segments following the 2023 Turkey earthquake doublet. With our stress-driven afterslip model, we derive the frictional parameters on each segment and predict the shallow slip rate till 2090. These allow us to investigate the relationship between creep, fault frictional properties, and earthquake ruptures.

2. Methods

To map the strain rate of EAFZ before the 2020 Elazığ and between the 2020 and 2023 Turkey earthquake doublet, we use long-term (1–3 years, with SAR images acquired in the same seasons) interferograms acquired in 2014–2020 and 2020–2023, respectively (Figures S1, S2, and Table S1 in Supporting Information S1). After testing different window sizes, a 1 km-by-1 km convolution filtering is used to extract the shallow slip signal from the wrapped interferograms, allowing for distracting the extremely high strain by stacking the phase gradients along the EAFZ (Text S1 in Supporting Information S1, Liu & Wang, 2023). With stacked phase gradients of the north-south and east-west direction from ascending and descending tracks, we resample them into the 300 m-by-300 m grid to calculate the shear strain rate in each patch along the fault under the assumption that the fault-normal motion is negligible. We also employ a phase-gradient-based time-series analysis (e.g., Cao et al., 2023) to probe the evolution of the afterslip following the 2023 earthquake doublet. Specifically, instead of using unwrapped phases, we insert the phase gradient of each interferogram to construct and calculate their time series in the Small Baseline Subset package (Morishita et al., 2020) (Figure S3 in Supporting Information S1). We use the line-of-sight (LOS) phase gradient in the north-south direction to represent the temporal evolution of the afterslip for the 2023 earthquake sequence.

The geometry and coseismic slip distribution of the 2020 Elazığ earthquake is from Pousse-Beltran et al. (2020) (Figure 1b). For the 2023 Kahramanmaraş earthquake doublet, we process the SAR and optical images from Sentinel-1/ALOS-2 and Sentinel-2 satellites, respectively, to derive the coseismic deformation (Text S1 and Figure S4 in Supporting Information S1). By tracing the surface ruptures, we assign 9 and 8 fault segments on the Mw7.8 and Mw7.6 earthquakes, respectively and inverse their fault geometries based on a Bayesian framework and Markov chain Monte Carlo method (Bagnardi & Hooper, 2018) (Figures S5 and S6 in Supporting Information S1). Then, we inverse the slips of 2 km-by-2 km subfaults on the determined fault planes to obtain the coseismic slip distribution (Figures 1a and 1c, Figures S7–S9 in Supporting Information S1). Note that from the source models, a ~50 km seismic gap is apparent on the Purtuge segment among these three earthquakes with little coseismic slip (Figures 1b and 1c).

We build a stress-driven afterslip model to simulate the afterslip of the 2023 Turkey earthquake doublets (Zhao & Yue, 2023), which is based on the steady-state RSF:

$$\tau = \sigma\left(f_0 + (a-b)\ln\left(\frac{v}{v_0}\right)\right) \quad (1)$$

Here, σ is the effective normal stress, v is the slip velocity of the fault, f_0 is the friction coefficient at the steady state velocity v_0, among which, $\sigma(a-b)$ and $R = \ln\left(\frac{v}{v_0}\right)$ are two critical parameters to characterize the velocity-dependence friction and initial stress changes. Given these parameters and the stress change induced by the earthquakes on each patch, we may simulate the time-series line-of-sight deformation on radar's acquisition dates to obtain simulated interferograms. Then, using the same filtering window and phase-gradient time-series method, we calculate the phase gradients to determine the optimal model parameters by comparing them with observations. Note that the stress-driven model is physical-based and thus different from kinematic afterslip models that fit the time-series deformation to an exponential curve.

3. Result

Shear-strain rates before the 2020 Elazığ earthquake clearly reveal several segments with extremely high values along the EAFZ, indicating the presence of aseismic shallow creeps (Figure 2a). Besides the well-known

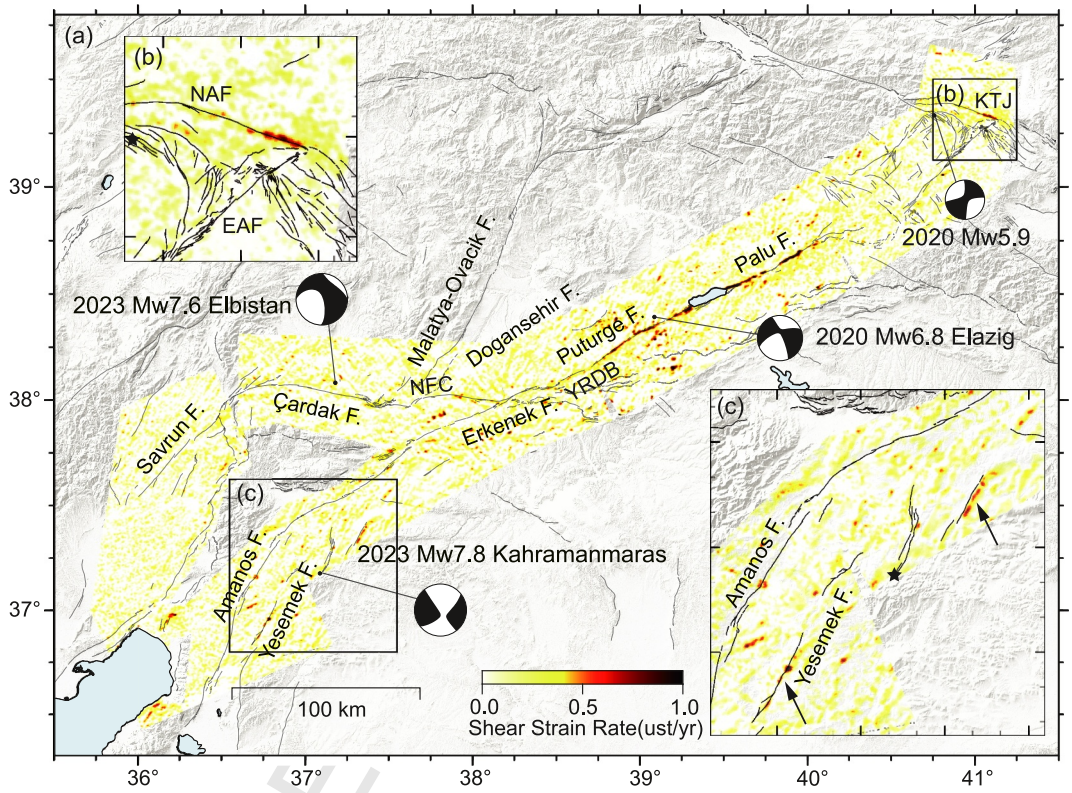

Figure 2. Shear-strain rates of the East Anatolian Fault Zone (EAFZ) between 2014 and 2020. NFC, Nurhak fault complex and YRDB, Yarpuzlu restraining double bend. (a) The shallow creep segment on the North Anatolian Fault around the Karliova Triple Junction. (b) Shallow creep segments on some secondary faults southwest of the EAFZ. "ust" means microstrain, used throughout this paper.

(~100 km) creeping Pütürge and Palu segments (Cakir et al., 2023), we identify several previously unknown strain-concentration segments. One segment is around the Karliova Triple Junction (Figure 2b), which may indicate the long-lasting afterslip of the 1949 M6.8 Karlıova earthquake. The other one is along some secondary faults paralleled with the Amanos Fault, for example, Yasemake Fault in the southwestern EAFZ (Figure 2c). However, the segments ruptured during the 2023 earthquake doublet exhibited no apparent strain-rate concentration, implying their shallow parts were mostly locked before 2020.

The 2020 Elazığ earthquake ruptured the central portion of the EAFZ, breaking nearly half of the Pütürge seismic gap, namely, the southwestern part of the creeping segment (Figures 2 and 3). Before the earthquake, the shear-strain rates were concentrated along the Pütürge fault to Palu, reaching up to 2 ust/yr on both sides of Lake Hazar (Figure 3a). West of the Lake, the 2020 earthquake occurred on a shear-strain gap between two ~15 km-long high-strain segments. Notably, no surface rupture was reported from InSAR observations imaged the affected area 3 days after the mainshock (Konca et al., 2021; Pousse-Beltran et al., 2020). The rupture terminated about 3 km below the surface, resulting in a shallow slip deficit of approximately 1 m (Cakir et al., 2023).

To probe how the earthquake affects the pre-existing shallow creep, we calculate the Coulomb stress change at 3 km depth with the EAF as the receiver fault (Toda et al., 2011) and compare it with the derived post-seismic shear-strain rates for the entire Pütürge segment (Figure 3b). The calculation is based on images acquired 7 months after the event to preclude the coseismic deformation of large aftershocks (Figure 3b). The derived shear-strain rates show that the spatial distribution of strain-concentrated regions along the fault extended significantly toward the southwest, with a shear-strain rate ~2 times greater than the pre-earthquake period. The extended and accelerated segments lay in the areas with positive coulomb stress changes. We find that maximum coseismic slips occurred on segments with relatively lower pre- and post-earthquake shear-strain rates than their adjacent counterparts (Figures 3c–3f).

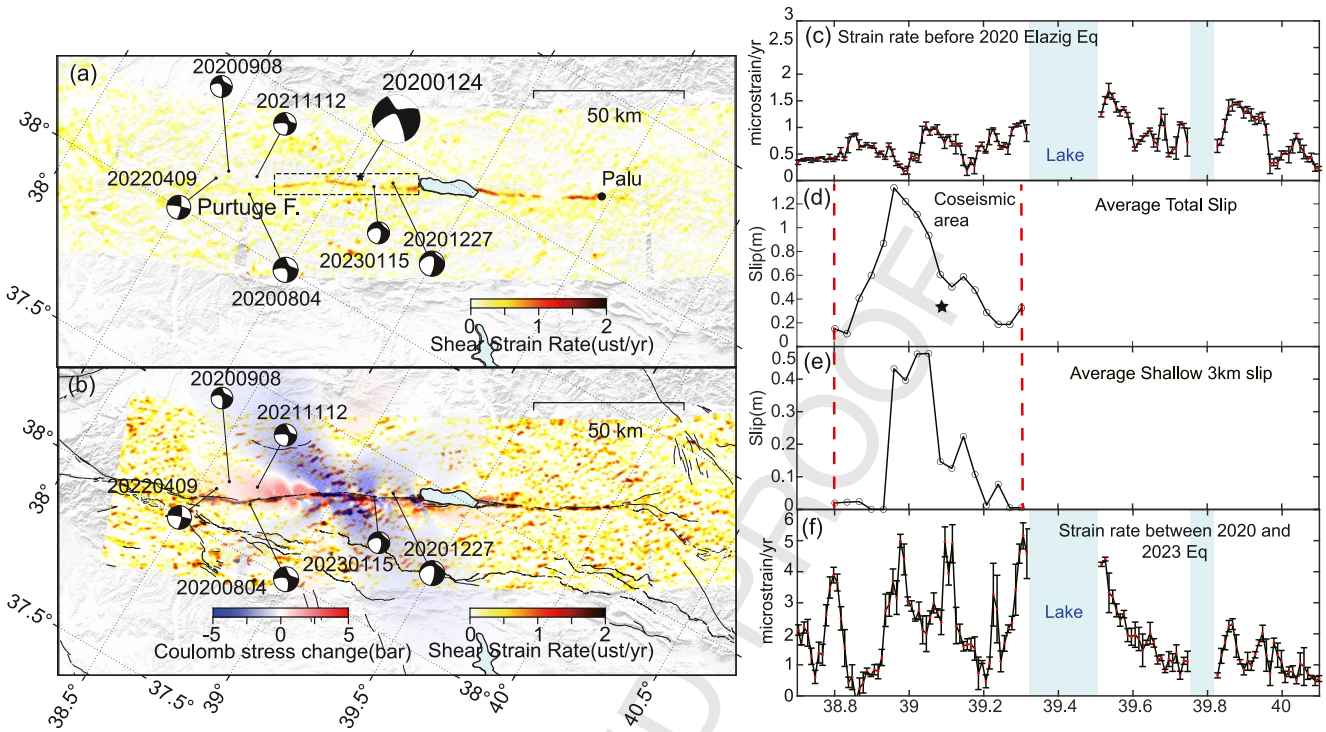

Figure 3. Shear-strain rates associated with the 2020 Mw 6.8 Elazığ earthquake. (a) Indicates the shear-strain rates before the earthquake. The dashed box indicates the area of the ruptured fault. (b) Indicates the shear-strain rates between August 2020 and January 2023 superimposed with the Coulomb stress changes caused by the earthquake. The beach balls show the mechanisms and epicenters of the main shock and aftershocks (over Mw 5.0) between February 2020 and January 2023. (c, f) Show the shear-strain rates with a 1 km interval on fault before and after the earthquake, respectively. (d, e) Show the total and shallow slip from the source model (Pousse-Beltran et al., 2020), respectively.

Three years after the 2020 Elazığ earthquake, the Mw 7.8 earthquake ruptured the main branch of the EAFZ, while the subsequent Mw 7.6 earthquake ruptured the northern branch of the EAFZ. From the shear strain rates before the earthquakes, we find no apparent shallow creep on both ruptured segments (Figure 3a). The shear-strain rates across the entire EAFZ from February 2023 to December 2023 provide a comprehensive view of how the shallowest part of faults behaves after the earthquakes (Figure 4b). Segments with high shear-strain rates appeared following the earthquakes, representing the triggered shallow afterslip. For the Mw 7.8 earthquake, the afterslip is concentrated at the northeastern end of the rupture, extending ~50 km along the Pütürge segment of the EAFZ. For the Mw 7.6 earthquake, the shallow afterslip has a total length of ~60 km along the Doğanşehir fault and around the Nurhak Fault Complex.

We sample profiles at intervals of 1 km along the fault both before and after the earthquake (Figures 4c–4h). By aligning the maximum shear-strain rates along the rupture, we also identify an evident compensation to the averaged coseismic slip of the uppermost 4 km depth. For the Mw 7.8 earthquake, the profile on the northeastern part of the segment shows that the afterslip is primarily concentrated on the S1 and half of the seismic gap between the 2020 and 2023 earthquake (Figure 1c), which has very limited shallow coseismic slip (<1 m) on the Pütürge segment (Figures 4c–4e). It means that the shallow portion of the middle Pütürge segment started to creep after the 2020 Mw 6.8 earthquake, and the Mw 7.8 earthquake accelerated it again, given the fact that all three earthquakes induced positive Coulomb stress changes on this segment (Figure 3 and Figure S10 in Supporting Information S1). For the Mw 7.6 earthquake, the afterslip is mainly located in segments S10 and S11. Notably, the averaged coseismic slip at the uppermost 4 km is much smaller in these two segments than in other segments to the west, with much larger shear-strain rates (Figures 4f–4h). Interestingly, on the Doğanşehir Fault, the strain rate concentrations form two peaks with lower rates in the middle, where an Mw 7.1 sub-event occurred during the Mw 7.6 earthquake (Jia et al., 2023) (Figure 4h).

Subsequently, the phase-gradient time series suggests that the strain rates were decaying in the two creeping segments with different temporal characteristics (Figure 5 and Figure S11 in Supporting Information S1). On the

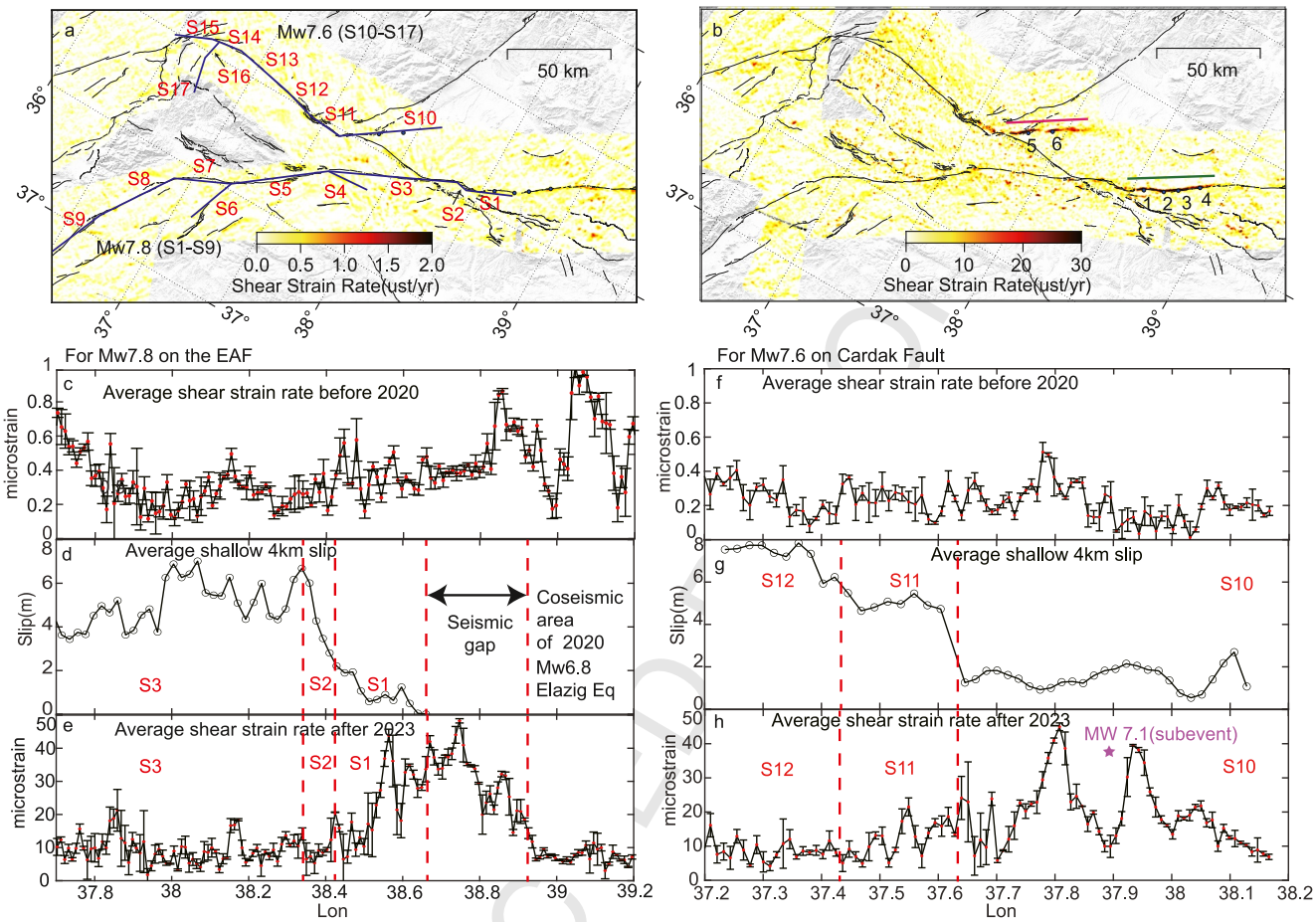

Figure 4. Shear-strain rates associated with the Mw 7.8 and Mw 7.6 Kahramanmaraş earthquake sequence. (a) Indicates the shear-strain rates before 2020 on the coseismic area of the 2023 sequence. Black solid lines represent the 17 segments of the coseismic slip model. (b) Indicates the shear-strain rates after the 2023 earthquake sequence. Magenta and green solid lines represent the approximate positions of the along-strike profiles below. Blue dots with numbers show the position of the selected points with time-series phase gradients shown in Figure 5. (c, e) And (f, h) show the shear-strain rate with a 1 km interval on fault before/after the Mw 7.8 earthquake on the main EAF and the Mw 7.6 earthquake on the Çardak fault, respectively. (d, g) Show the average shallow slip (4 km) of the Mw 7.8 and Mw 7.6 earthquakes, respectively.

Pütürge segment (points 1–4 in Figures 5a and 5b), hosting the Mw 7.8 earthquake, the phase gradients decayed relatively slowly, maintaining a rapid creep rate till January 2024. Notably, points 2 and 3, located near the Yarpuzlu restraining double bend, maintained high rates since the earthquake. On the Doğanşehir segment (points 5 and 6 in Figures 5c and 5d) hosting the Mw 7.6 earthquake, the phase gradients decayed more rapidly, reaching a relatively low rate after September 2023.

We then use a stress-driven model to simulate the shallow afterslip on each SAR acquisition date and search for parameters that can reproduce the observed time series of LOS phase gradients (Figures S12–S15 in Supporting Information S1). The best-fiting model shows that the fault frictional properties ($\sigma(a-b)$) and pre-earthquake slip rate (V_{pre}) in the afterslip regions of the two earthquakes differ significantly. Note that V_{pre} is different from v_0 in Equation 1 (Wang & Bürgmann, 2020, Text S1 in Supporting Information S1). Also, we assume the same $\sigma(a-b)$ and V_{pre} on all fault patches of the two segments and the value of the coseismic stress change on the fault plane is shown in Figure S17 in Supporting Information S1. Along the main segment of the EAF, the Pütürge segment exhibited higher $\sigma(a-b) \approx 0.7$ MPa and $V_{pre} = 6 \times 10^{-9}$ m/s, which indicates a faster decay on the afterslip, while the Doğanşehir segment has lower $\sigma(a-b) \approx 0.4$ MPa and $V_{pre} = 3 \times 10^{-9}$ m/s (Figures 5a–5d). By applying these parameters, the stress-driven afterslip model predicts that the Pütürge segment will maintain a relatively fast shallow slip with the rate of ~10 mm/yr for decades to come. In comparison, the Doğanşehir segment will decay to a relatively slow shallow slip rate of about 3 mm/yr (Text S1 in Supporting Information S1).

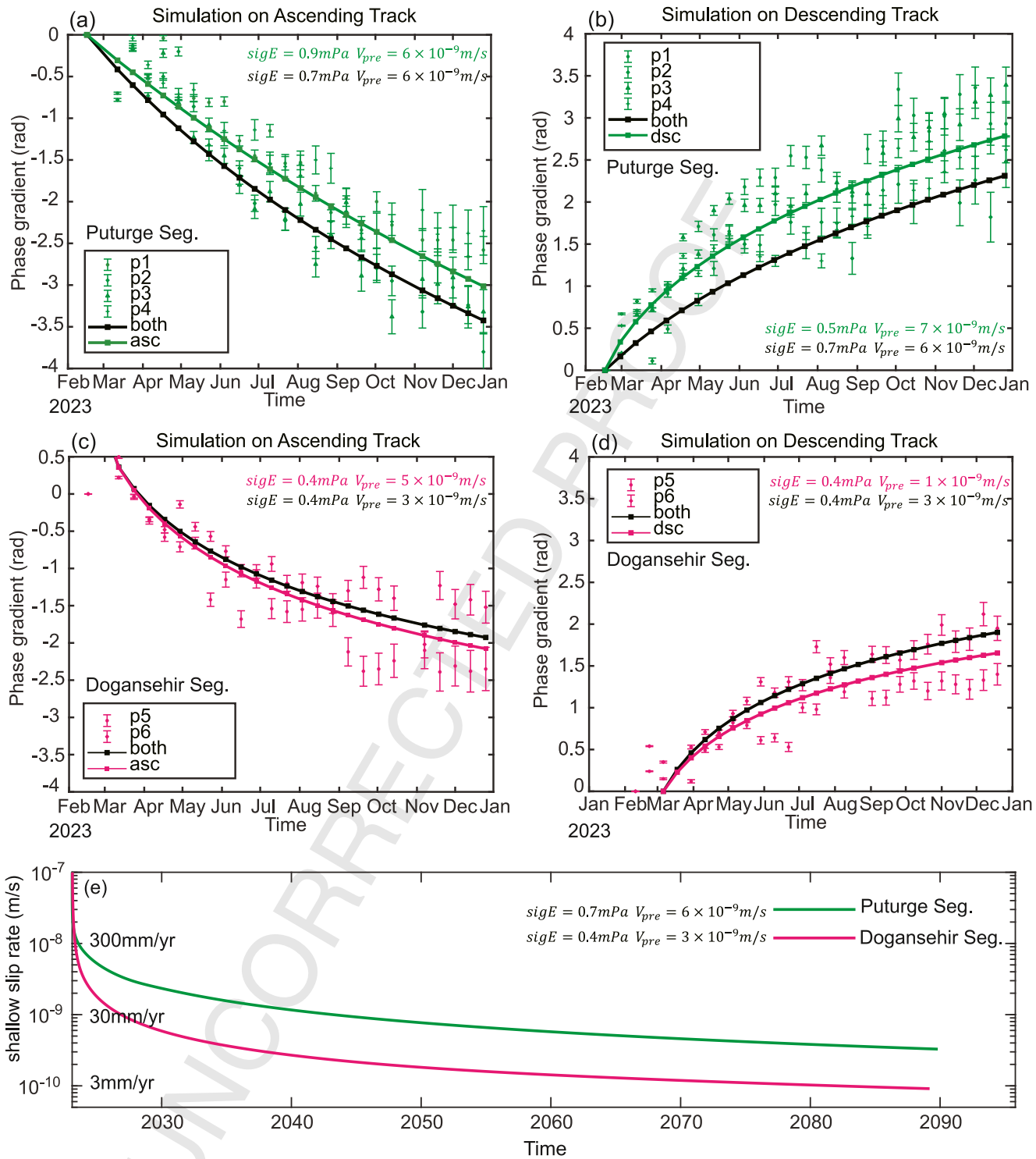

Figure 5. The temporal evolution of the line-of-sight phase gradients on points 1–6 (Figure 4) after the 2023 earthquake sequence simulated from the stress-driven afterslip models. (a, b) Show the time-series phase gradients on the Pütürge segment for the Mw 7.8 earthquake (points 1–4) for ascending track 116 and descending track 123, respectively. (c, d) Are the time-series phase gradients on the Doğanşehir segment for the Mw 7.6 earthquake (points 5–6) for ascending track 116 and descending track 21, respectively. Black solid lines represent simulations with best fits on both ascending and descending tracks. Green and magenta lines separately represent the best-fit simulation on the Pütürge segment and Doğanşehir segment, respectively. (e) Shows the simulated long-term shallow slips (within the 2 km uppermost crust) of each segment.

4. Discussion and Conclusion

The shear-strain rates spanning the three recent earthquakes in the EAFZ show that the creep on the EAFZ is tightly related to the amounts of shallow coseismic slips. Specifically, the 2020 Elazığ earthquake initiated on the previous creeping segment yet in the strain-rate shadow. The earthquake did not rupture to the surface but expanded (20 km westwards) and accelerated the creeps west of the Lake Hazar. The 2023 Mw 7.8 and Mw 7.6 earthquakes occurred on the previously non-creeping fault, but the earthquakes triggered creeps on the tips of coseismic ruptures with obvious shallow slip deficits. Interestingly, the shallow creep on the 50 km Purtuge seismic gap accelerated two times by the 2020 Elazığ and 2023 Kahramanmaraş earthquakes.

By comparing the shear strain rate of the EAFZ before and after the three earthquakes, and the coseismic slip distribution inverted using geodetic observations, we show that the creep before the earthquake strongly affects the magnitudes of coseismic slips. It is consistent with the conclusion that all five shallowly creeping segments on the NAF are located along earthquake ruptures with relatively lower slip (Liu & Wang, 2023). Furthermore, the newly obtained shear-strain changes suggest that earthquakes can also accelerate the creeping rate and extend the spatial distribution of the pre-existing creep segments. A similar scenario may happen on the Ismetpasa creeping segment of the NAF, which has kept creeping since the 1944 earthquake (Cakir et al., 2005). It was further influenced by the 1951 earthquake, which produced a shear strain-rate shadow in the segment (Liu & Wang, 2023), similar to the observed strain-rate shadow caused by the Mw 7.1 subevent on the Çardak segment. These discoveries highlight that earthquakes are essential in adjusting creeping segments' spatial and temporal behavior.

The proposed phase-gradient time-series analysis provides a new approach to investigating the strain evolution due to very shallow slips near the fault (∼1 km). With the advantage of the high resolution and sensitivity to the short-wavelength signal, InSAR phase gradients can be used to derive high-resolution strain rates and shallow strain series with high temporal resolution. This is particularly useful when applied to wrapped interferograms shortly acquired after the earthquake. As for the 2023 earthquake sequence, implementing the deformation-based methods is a challenge due to the strong tropospheric turbulence and unwrapping errors (Figure S16 in Supporting Information S1).

The stress-driven afterslip model reveals that the heterogeneity of the frictional properties and the difference of the coseismic stress change on the fault may result in different temporal characteristics of fault creeps. The model provides evidence that the afterslip may last a long time (>50 years), maintaining a slip rates at the level of tectonic loading, similar to the creep on the Izmit (maximum ∼12 mm/yr) (Aslan et al., 2019; Özarpacı et al., 2021) and the Ismetpasa segment (∼8 mm/yr) (Rousset et al., 2016) of the NAF after the 1999 Izmit and 1944 earthquakes, respectively. Also, fault creep has been identified on the Laohushan segment (∼3 mm/yr) (Ou et al., 2022) of the Haiyuan fault and on the Ganzi-Yushu fault (∼6 mm/yr) (Cai et al., 2024), associated with the 1920 Haiyuan and 2010 Yushu earthquakes, respectively. Our simulation shows that the creep triggered by earthquakes can remain high rates for decades with large $\sigma(a-b)$, though tectonic loading may also play a role by providing long-term driving forces in the interseismic stage. In summary, the stress-driven afterslip model illustrates the joint control of coseismic stress changes, fault friction parameters, and pre-earthquake slip velocities on initiating new creeps, confirming that earthquake-induced afterslip may potentially transition into long-lasting creep.

To conclude, by applying the InSAR phase-gradient-based method, we derive the high-resolution shear-strain rates spanning three earthquakes from 2014 to 2023 on the entire EAFZ. We find that earthquakes can extend and accelerate pre-existing creeps on faults. Earthquakes and shallow creeps tend to release the strain on different portions of faults. More importantly, we reveal that proper coseismic stress changes and frictional properties may stimulate long-lasting creeps on strike-slip faults that can be explained by a physical-based stress-driven model. As future work, long-term observation, rock experiments and more research on other strike-slip faults are required to further verify our understanding of fault creep in the earthquake cycle.

Data Availability Statement

All data used in this study is open-access. The SAR images from Sentinel-1 A/B were downloaded from the European Space Agency (ESA, https://dataspace.copernicus.eu/), with copies hosted at Alaska SAR Facility

(ASF, https://asf.alaska.edu). Data providers require user registration to gain access. The earthquake catalogs and focal mechanism solutions are available at Global Centroid Moment-Tensor (CMT) Project (https://www.globalcmt.org/CMTsearch.html) and Kandilli Observatory and Earthquake Research Institute of Bogazici University (http://www.koeri.boun.edu.tr/sismo/2/earthquake-catalog/) (KOERI, 1971). The time series analysis software LiCSBAS can be accessed via Morishita et al. (2020). The gradient data of each track and the shear strain rates of each patch are available via Liu et al. (2024). The figures in this study were generated using the public Generic Mapping Tools (GMT) (Wessel et al., 2013).

Acknowledgments
Sentinel-1 SAR data are provided by the European Space Agency and are additionally distributed by the Alaska Satellite Facility. This work is funded by the National Natural Science Foundation of China (42021003). Ziming Liu would like to express gratitude to the China Scholarship Council (CSC) for providing financial support during the study and research abroad.

References

Aslan, G., Lasserre, C., Cakir, Z., Ergintav, S., Özarpaci, S., Dogan, U., et al. (2019). Shallow creep along the 1999 Izmit earthquake rupture (Turkey) from GPS and high temporal resolution interferometric synthetic aperture radar data (2011–2017). *Journal of Geophysical Research: Solid Earth*, *124*(2), 2218–2236. https://doi.org/10.1029/2018JB017022

Bagnardi, M., & Hooper, A. (2018). Inversion of surface deformation data for rapid estimates of source parameters and uncertainties: A Bayesian approach. *Geochemistry, Geophysics, Geosystems*, *19*(7), 2194–2211. https://doi.org/10.1029/2018GC007585

Bilham, R., Ozener, H., Mencin, D., Dogru, A., Ergintav, S., Cakir, Z., et al. (2016). Surface creep on the North Anatolian Fault at Ismetpasa, Turkey, 1944–2016. *Journal of Geophysical Research: Solid Earth*, *121*(10), 7409–7431. https://doi.org/10.1002/2016JB013394

Cai, J., Wen, Y., He, K., Wang, X., & Xu, C. (2024). Strain partitioning, interseismic coupling, and shallow creep along the Ganzi-Yushu fault from Sentinel-1 InSAR data. *Geophysical Research Letters*, *51*(21), e2024GL111469. https://doi.org/10.1029/2024GL111469

Cakir, Z., Akoglu, A. M., Belabbes, S., Ergintav, S., & Meghraoui, M. (2005). Creeping along the Ismetpasa section of the North Anatolian Fault (western Turkey): Rate and extent from InSAR. *Earth and Planetary Science Letters*, *238*(1), 225–234. https://doi.org/10.1016/j.epsl.2005.06.044

Cakir, Z., Doğan, U., Akoğlu, A. M., Ergintav, S., Özarpacı, S., Özdemir, A., et al. (2023). Arrest of the Mw 6.8 January 24, 2020 Elaziğ (Turkey) earthquake by shallow fault creep. *Earth and Planetary Science Letters*, *608*, 118085. https://doi.org/10.1016/j.epsl.2023.118085

Cakir, Z., Ergintav, S., Ozener, H., Dogan, U., Akoglu, A. M., Meghraoui, M., & Reilinger, R. (2012). Onset of aseismic creep on major strike-slip faults. *Geology*, *40*(12), 1115–1118. https://doi.org/10.1130/G33522.1

Cao, Y., Hamling, I., Massey, C., & Upton, P. (2023). Slow-moving landslides triggered by the 2016 Mw 7.8 Kaikōura earthquake, New Zealand: A new InSAR phase-gradient based time-series approach. *Geophysical Research Letters*, *50*(4), e2022GL102064. https://doi.org/10.1029/2022GL102064

Cavalié, O., Lasserre, C., Doin, M.-P., Peltzer, G., Sun, J., Xu, X., & Shen, Z.-K. (2008). Measurement of interseismic strain across the Haiyuan fault (Gansu, China), by InSAR. *Earth and Planetary Science Letters*, *275*(3–4), 246–257. https://doi.org/10.1016/j.epsl.2008.07.057

Cetin, E., Cakir, Z., Meghraoui, M., Ergintav, S., & Akoglu, A. M. (2014). Extent and distribution of aseismic slip on the Ismetpaşa segment of the North Anatolian Fault (Turkey) from persistent scatterer InSAR. *Geochemistry, Geophysics, Geosystems*, *15*(7), 2883–2894. https://doi.org/10.1002/2014GC005307

Dieterich, J. H. (1979). Modeling of rock friction: 1. Experimental results and constitutive equations. *Journal of Geophysical Research*, *84*(B5), 2161–2168. https://doi.org/10.1029/JB084iB05p02161

Duman, T. Y., & Emre, Ö. (2013). The East Anatolian Fault: Geometry, segmentation and jog characteristics. *Geological Society, London, Special Publications*, *372*(1), 495–529. https://doi.org/10.1144/SP372.14

Emre, O., Duman, T., Özalp, S., Elmaci, H., Olgun, Ş., & Şaroğlu, F. (2013). Active fault map of Turkey with an explanatory text.

England, P., Houseman, G., & Nocquet, J.-M. (2016). Constraints from GPS measurements on the dynamics of deformation in Anatolia and the Aegean. *Journal of Geophysical Research: Solid Earth*, *121*(12), 8888–8916. https://doi.org/10.1002/2016JB013382

Ezgi Güvercin, S. (2024). 2023 earthquake doublet in Türkiye reveals the complexities of the East Anatolian Fault Zone: Insights from aftershock patterns and moment tensor solutions. *Seismological Research Letters*, *95*(2A), 664–679. https://doi.org/10.1785/0220230317

Harris, R. A. (2017). Large earthquakes and creeping faults. *Reviews of Geophysics*, *55*(1), 169–198. https://doi.org/10.1002/2016RG000539

Hussain, E., Wright, T. J., Walters, R. J., Bekaert, D., Hooper, A., & Houseman, G. A. (2016). Geodetic observations of postseismic creep in the decade after the 1999 Izmit earthquake, Turkey: Implications for a shallow slip deficit: IZMIT CREEP. *Journal of Geophysical Research: Solid Earth*, *121*(4), 2980–3001. https://doi.org/10.1002/2015JB012737

Jia, Z., Jin, Z., Marchandon, M., Ulrich, T., Gabriel, A.-A., Fan, W., et al. (2023). The complex dynamics of the 2023 Kahramanmaraş, Turkey, Mw 7.8-7.7 earthquake doublet. *Science*, *381*(6661), 985–990. https://doi.org/10.1126/science.adi0685

Jolivet, R., Lasserre, C., Doin, M.-P., Guillaso, S., Peltzer, G., Dailu, R., et al. (2012). Shallow creep on the Haiyuan Fault (Gansu, China) revealed by SAR interferometry. *Journal of Geophysical Research*, *117*(B6), B06401. https://doi.org/10.1029/2011JB008732

Jolivet, R., Simons, M., Agram, P. S., Duputel, Z., & Shen, Z.-K. (2015). Aseismic slip and seismogenic coupling along the central San Andreas Fault. *Geophysical Research Letters*, *42*(2), 297–306. https://doi.org/10.1002/2014GL062222

Kandilli Observatory and Earthquake Research Institute, Boğaziçi University. (1971). Kandilli Observatory and Earthquake Research Institute (KOERI) [Dataset]. *International Federation of Digital Seismograph Networks*. https://doi.org/10.7914/SN/KO

Karabulut, H., Ezgi, G. S., James, H., & Ali Özgün, K. (2023). Long silence on the East Anatolian Fault Zone (Southern Turkey) ends with devastating double earthquakes (6 February 2023) over a seismic gap: Implications for the seismic potential in the Eastern Mediterranean region. *Journal of the Geological Society*, *180*(3). https://doi.org/10.1144/jgs2023-021

Konca, A. Ö., Karabulut, H., Güvercin, S. E., Eskiköy, F., Özarpacı, S., Özdemir, A., et al. (2021). From interseismic deformation with near-repeating earthquakes to co-seismic rupture: A unified view of the 2020 Mw6.8 Sivrice (Elazığ) eastern Turkey earthquake. *Journal of Geophysical Research: Solid Earth*, *126*(10), e2021JB021830. https://doi.org/10.1029/2021JB021830

Langbein, J., Murray, J. R., & Snyder, H. A. (2006). Coseismic and initial postseismic deformation from the 2004 Parkfield, California, earthquake, observed by global positioning system, electronic distance meter, creepmeters, and borehole strainmeters. *Bulletin of the Seismological Society of America*, *96*(4B), S304–S320. https://doi.org/10.1785/0120050823

Liu, Z., Luo, H., Klinger, Y., & Wang, T. (2024). Data for "shear strain evolution spanning the 2020 Mw6.8 Elazığ and 2023 Mw7.8/Mw7.6 Kahramanmaraş earthquake sequence along the East Anatolian Fault Zone" manuscript [Dataset]. *Zenodo*. https://doi.org/10.5281/zenodo.14010311

Liu, Z., & Wang, T. (2023). High-resolution interseismic strain mapping from InSAR phase-gradient stacking: Application to the North Anatolian Fault with implications for the non-uniform strain distribution related to coseismic slip distribution. *Geophysical Research Letters*, *50*(15), e2023GL104168. https://doi.org/10.1029/2023GL104168

Lomax, A. (2023). Precise, NLL-SSST-coherence hypocenter catalog for the 2023 Mw 7.8 and Mw 7.6 SE Turkey earthquake sequence. (v3.0) [Dataset]. *Zenodo*. https://doi.org/10.5281/zenodo.8089273

Melgar, D., Ganas, A., Taymaz, T., Valkaniotis, S., Crowell, B. W., Kapetanidis, V., et al. (2020). Rupture kinematics of 2020 January 24 Mw 6.7 Doğanyol-Sivrice, Turkey earthquake on the East Anatolian Fault Zone imaged by space geodesy. *Geophysical Journal International*, *223*(2), 862–874. https://doi.org/10.1093/gji/ggaa345

Morishita, Y., Lazecky, M., Wright, T. J., Weiss, J. R., Elliott, J. R., & Hooper, A. (2020). LiCSBAS: An open-source InSAR time series analysis package integrated with the LiCSAR automated Sentinel-1 InSAR processor. *Remote Sensing*, *12*(3), 424. https://doi.org/10.3390/rs12030424

Ou, Q., Daout, S., Weiss, J. R., Shen, L., Lazecký, M., Wright, T. J., & Parsons, B. E. (2022). Large-scale interseismic strain mapping of the NE Tibetan Plateau from Sentinel-1 interferometry. *Journal of Geophysical Research: Solid Earth*, *127*(6), e2022JB024176. https://doi.org/10.1029/2022JB024176

Özarpacı, S., Doğan, U., Ergintav, S., Çakır, Z., Özdemir, A., Floyd, M., & Reilinger, R. (2021). Present GPS velocity field along 1999 Izmit rupture zone: Evidence for continuing afterslip 20 yr after the earthquake. *Geophysical Journal International*, *224*(3), 2016–2027. https://doi.org/10.1093/gji/ggaa560

Perfettini, H., & Avouac, J.-P. (2004). Postseismic relaxation driven by brittle creep: A possible mechanism to reconcile geodetic measurements and the decay rate of aftershocks, application to the Chi-Chi earthquake, Taiwan. *Journal of Geophysical Research*, *109*(B2), B02304. https://doi.org/10.1029/2003JB002488

Pousse-Beltran, L., Nissen, E., Bergman, E. A., Cambaz, M. D., Gaudreau, É., Karasözen, E., & Tan, F. (2020). The 2020 Mw 6.8 Elazığ (Turkey) earthquake reveals rupture behavior of the East Anatolian Fault. *Geophysical Research Letters*, *47*(13), e2020GL088136. https://doi.org/10.1029/2020GL088136

Provost, F., Karabacak, V., Malet, J.-P., Van der Woerd, J., Meghraoui, M., Masson, F., et al. (2024). High-resolution co-seismic fault offsets of the 2023 Türkiye earthquake ruptures using satellite imagery. *Scientific Reports*, *14*(1), 6834. https://doi.org/10.1038/s41598-024-55009-5

Reilinger, R., McClusky, S., Vernant, P., Lawrence, S., Ergintav, S., Cakmak, R., et al. (2006). GPS constraints on continental deformation in the Africa-Arabia-Eurasia continental collision zone and implications for the dynamics of plate interactions. *Journal of Geophysical Research*, *111*(B5), B05411. https://doi.org/10.1029/2005JB004051

Ren, C., Wang, Z., Taymaz, T., Hu, N., Luo, H., Zhao, Z., et al. (2024). Supershear triggering and cascading fault ruptures of the 2023 Kahramanmaraş, Türkiye, earthquake doublet. *Science*, *383*(6680), 305–311. https://doi.org/10.1126/science.adi1519

Rousset, B., Jolivet, R., Simons, M., Lasserre, C., Riel, B., Milillo, P., et al. (2016). An aseismic slip transient on the North Anatolian Fault. *Geophysical Research Letters*, *43*(7), 3254–3262. https://doi.org/10.1002/2016GL068250

Ruina, A. (1983). Slip instability and state variable friction laws. *Journal of Geophysical Research*, *88*(B12), 10359–10370. https://doi.org/10.1029/JB088iB12p10359

Scholz, C. H. (1998). Earthquakes and friction laws. *Nature*, *391*(6662), 37–42. https://doi.org/10.1038/34097

Steinbrugge, K. V., Zacher, E. G., Tocher, D., Whitten, C. A., & Claire, C. N. (1960). Creep on the San Andreas Fault. *Bulletin of the Seismological Society of America*, *50*(3), 389–415. https://doi.org/10.1785/BSSA0500030389

Taymaz, T., Westaway, R., & Reilinger, R. (2004). Active faulting and crustal deformation in the Eastern Mediterranean region. *Tectonophysics*, *391*(1), 1–9. https://doi.org/10.1016/j.tecto.2004.07.005

Toda, S., Stein, R. S., Sevilgen, V., & Lin, J. (2011). Coulomb 3.3 graphic-rich deformation and stress-change software for earthquake, tectonic, and volcano research and teaching—user guide. *U.S. Geological Survey Open-File Report 2011–1060*, *63*(7), 725–730. https://doi.org/10.5047/eps.2011.05.010

Wang, K., & Bürgmann, R. (2020). Probing fault frictional properties during afterslip updip and downdip of the 2017 Mw 7.3 Sarpol-e Zahab earthquake with space geodesy. *Journal of Geophysical Research: Solid Earth*, *125*(11), e2020JB020319. https://doi.org/10.1029/2020JB020319

Wessel, P., Smith, W. H. F., Scharroo, R., Luis, J., & Wobbe, F. (2013). Generic mapping tools: Improved version released. *Eos, Transactions American Geophysical Union*, *94*(45), 409–410. https://doi.org/10.1002/2013eo450001

Zhang, Y., Tang, X., Liu, D., Taymaz, T., Eken, T., Guo, R., et al. (2023). Geometric controls on cascading rupture of the 2023 Kahramanmaraş earthquake doublet. *Nature Geoscience*, *16*(11), 1054–1060. https://doi.org/10.1038/s41561-023-01283-3

Zhao, Z., & Yue, H. (2023). A two-step inversion for fault frictional properties using a temporally varying afterslip model and its application to the 2019 Ridgecrest earthquake. *Earth and Planetary Science Letters*, *602*, 117932. https://doi.org/10.1016/j.epsl.2022.117932

References From the Supporting Information

Barbot, S., Fialko, Y., & Bock, Y. (2009). Postseismic deformation due to the Mw 6.0 2004 Parkfield earthquake: Stress-driven creep on a fault with spatially variable rate-and-state friction parameters. *Journal of Geophysical Research*, *114*(B7), B07405. https://doi.org/10.1029/2008JB005748

Chen, C. W., & Zebker, H. A. (2000). Network approaches to two-dimensional phase unwrapping: Intractability and two new algorithms. *Journal of the Optical Society of America A*, *17*(3), 401–414. https://doi.org/10.1364/josaa.17.000401

Fialko, Y., Simons, M., & Agnew, D. (2001). The complete (3-D) surface displacement field in the epicentral area of the 1999 MW7.1 Hector Mine Earthquake, California, from space geodetic observations. *Geophysical Research Letters*, *28*(16), 3063–3066. https://doi.org/10.1029/2001gl013174

Goldstein, R. M., & Werner, C. L. (1998). Radar interferogram filtering for geophysical applications. *Geophysical Research Letters*, *25*(21), 4035–4038. https://doi.org/10.1029/1998gl900033

Jonsson, S. O., Zebker, H., Segall, P., & Falk, A. (2002). Fault slip distribution of the 1999 Mw7.1 Hector Mine, California, earthquake, estimated from satellite radar and GPS measurements. *Bulletin of the Seismological Society of America*, *92*(4), 1377–1389. https://doi.org/10.1785/0120000922

Liang, C., Agram, P., Simons, M., & Fielding, E. J. (2019). Ionospheric correction of InSAR time series analysis of C-band Sentinel-1 TOPS data. *IEEE Transactions on Geoscience and Remote Sensing*, *57*(9), 6755–6773. https://doi.org/10.1109/tgrs.2019.2908494

Okada, Y. (1985). Surface deformation due to shear and tensile faults in a half-space. *Bulletin of the Seismological Society of America*, *75*(4), 1135–1154. https://doi.org/10.1785/bssa0750041135

Wang, R., Schurr, B., Milkereit, C., Shao, Z., & Jin, M. (2011). An improved automatic scheme for empirical baseline correction of digital strong-motion records. *Bulletin of the Seismological Society of America*, *101*(5), 2029–2044. https://doi.org/10.1785/0120110039

Wang, T., & Jonsson, S. (2015). Improved SAR amplitude image offset measurements for deriving three-dimensional coseismic displacements. In *IEEE Journal of selected topics in applied Earth observations and remote sensing* (Vol. 8, No. (7), pp. 3271–3278). https://doi.org/10.1109/jstars.2014.2387865